High-Temperature Equation of State of FeH: Implications for Hydrogen in Earth's Inner Core

Shoh Tagawa[1], Hitoshi Gomi[1], Kei Hirose[2], and Yasuo Ohishi[3]

[1]Tokyo Institute of Technology
[2]The University of Tokyo
[3]Japan Synchrotron Radiation Research Institute

November 23, 2022

Abstract

While hydrogen is one of plausible major light elements in the core, the high-temperature equation of state (EoS) of Fe-H alloy has not been experimentally examined to the core pressure range. Here we measured the volume (V) of non-magnetic (NM) fcc FeH at high pressure and temperature (P-T) to 142 GPa and 3660 K in a laser-heated diamond-anvil cell (DAC) and obtained its P-V-T EoS. An increase in the lattice volume of Fe per H atom, ΔVH, determined as functions of P and T is found to be substantially smaller than the volume of metallic H that has been used to estimate H concentration in Fe-H alloy. The ΔVH is almost identical between fcc and dhcp phases in the NM state, suggesting that it is applicable to hcp. The extrapolation of ΔVH to inner core conditions indicates its maximum H content to be 0.8–0.9 wt%.

High-Temperature Equation of State of FeH: Implications for Hydrogen in Earth's Inner Core

Shoh Tagawa[1,2], Hitoshi Gomi[1], Kei Hirose[1,2], and Yasuo Ohishi[3]

[1]Earth-Life Science Institute, Tokyo Institute of Technology, Tokyo, Japan
[2]Department of Earth and Planetary Science, The University of Tokyo, Tokyo, Japan
[3]Japan Synchrotron Radiation Research Institute, SPring-8, Hyogo, Japan

Correspondence to: S. Tagawa (shoh@elsi.jp)

Key Points:

- We obtained the *P*-*V*-*T* equation of state of FeH based on volume measurements up to 142 GPa and 3660 K using a diamond-anvil cell.
- ΔV_H, the volume increase of Fe by H atom, was determined as functions of *P* and *T*, enabling estimates of the H content in non-magnetic FeH*x*.
- We estimate the maximum H content in the inner core and discuss the possible compositional range of the Fe-H-Si-S inner core.

Abstract While hydrogen is one of plausible major light elements in the core, the high-temperature equation of state (EoS) of Fe-H alloy has not been experimentally examined to the core pressure range. Here we measured the volume (*V*) of non-magnetic (NM) fcc FeH at high pressure and temperature (*P*-*T*) to 142 GPa and 3660 K in a laser-heated diamond-anvil cell (DAC) and obtained its *P*-*V*-*T* EoS. An increase in the lattice volume of Fe per H atom, ΔV_H, determined as functions of *P* and *T* is found to be substantially smaller than the volume of metallic H that has been used to estimate H concentration in Fe-H alloy. The ΔV_H is almost identical between fcc and dhcp phases in the NM state, suggesting that it is applicable to hcp. The extrapolation of ΔV_H to inner core conditions indicates its maximum H content to be 0.8–0.9 wt%.

Plain Language Summary FeH is an important component in terrestrial planetary cores, and its EoS is useful to estimate their H concentrations from densities. The high-*T*

EoS of FeH has not been examined experimentally to the Earth's core pressure range (>136 GPa) because of difficulties in high *P-T* experiments on H-bearing systems. The fcc (face-centered-cubic) structure is known to be a stable form of FeH under a wide *P-T* range. Also, our first-principles calculations show that fcc FeH loses the local spin moment with increasing pressure to ~40 GPa. In the present experiments, we determined the volume of fcc FeH to 142 GPa and 3660 K and obtained its EoS for the NM state based on data collected above 41 GPa. The lattice volume of Fe expands by incorporating H in its interstitial site. Our data show that ΔV_H, the volume increase per H atom, is independent on the crystal structure of FeH in the absence of magnetism. Such ΔV_H obtained as functions of *P* and *T* in this study predicts the density of FeH*x* ($x < 1$) under inner core conditions. These results give the possible compositional range of the Fe-H-Si-S inner core.

1. Introduction

Hydrogen could be one of major light elements in planetary iron cores and has attracted much attention recently (see Hirose et al., 2021 for a review). Recent experimental and computational studies of metal-silicate partitioning of H showed that a large amount of H equivalent to that in 30–70 times Earth's ocean mass of water could have been distributed into the core during its formation (Tagawa et al., 2021; Li et al., 2020; Yuan & Steinle-Neumann, 2020). Indeed, the density and seismic velocity of both the outer and inner core can be reconciled with H-rich Fe alloys (Umemoto & Hirose, 2015, 2020; Wang et al., 2021). In addition, recent seismic observations of the Martian core indicate that its density is relatively low, possibly suggesting the presence of 1–2 wt% H (Stähler et al., 2021). Hydrogen in the cores of such terrestrial planets may have derived from water that was transported from an outer region of the solar system (Raymond & Morbidelli, 2020) and from proto-solar nebular gas (Ikoma & Genda, 2006; Olson & Sharp, 2019). The amount of H in the core is a key to better understanding the processes of planetary formation.

In order to constrain the H content in metallic cores, the EoS of Fe-H alloy is of great importance. While it has been reported by theory to inner core conditions (Caracas, 2015), its experimental determination has been challenging because 1) Fe has negligible solubility of H at 1 bar (e.g., Fukai & Suzuki, 1986) and 2) H concentration in Fe-H alloy therefore needs to be estimated under pressure. The EoS of stoichiometric FeH has been examined by X-ray diffraction (XRD) measurements under high pressure but only at room temperature (Badding et al., 1991; Hirao et al., 2004; Narygina et al., 2011; Pépin et al., 2014; Kato et al., 2020), except for multi-anvil experiments performed up to 21

GPa and 1573 K (Sakamaki et al., 2009). The EoSs obtained by these earlier studies differ from each other because of the differences in crystal structure (double hexagonal-close-packed, dhcp and fcc) and magnetic state (ferromagnetic, FM and NM).

The volume increase of Fe per H atom, ΔV_H, provides the density of an Fe-H alloy since the lattice volume of iron expands proportionally to the amount of H (Caracas, 2015). In addition, the ΔV_H has been widely used to estimate H concentration in Fe-H alloys (Fukai, 1992; Thompson et al., 2018; Tagawa et al., 2021). Originally Fukai (1992) employed ΔV_H from the volume of metallic H (Chakravarty et al., 1981). Recent neutron diffraction measurements directly gave ΔV_H at high *P-T* (Machida et al., 2014, 2019; Ikuta et al., 2019), but the pressure range for such neutron diffraction studies has been limited to 12 GPa, much lower than Earth's core conditions. The temperature effect on ΔV_H remains primarily unknown (Wang et al., 2021).

In this study, we examined fcc stoichiometric FeH at high *P-T* based on experiment and theory. The thermal EoS is obtained for the NM state by measuring the volume up to 146 GPa/300 K and 119 GPa/3720 K in a laser-heated DAC. By comparing its volume with that of pure Fe, we obtain ΔV_H (P, T) as functions of P and T and discuss H concentration in the Earth's inner core. Such ΔV_H (P, T) is also useful to estimate the H content in Fe-H alloys in-situ at high *P-T*.

2. Methods

2.1. Experiments

High *P-T* experiments were performed in a laser-heated DAC (Figure 1a, 1b). Three separate runs were carried out using beveled anvils with 120 and 300 μm culet sizes. A Re gasket was preindented to about 25 μm thick. Sample configuration was similar to that in Tagawa et al. (2016). In order to prevent hydrogen loss to the Re gasket, we employed a NaCl inner gasket prepared with a Focused Ion Beam. The surface of the diamond anvils was coated with a thin layer of Ti by sputtering (Ohta et al., 2015). We loaded a ~10 μm thick pure Fe foil (>99.999% purity, Toho Zinc) being sandwiched by thin NaCl plates that were used as a pressure marker. Only in run #3, a KCl pellet was placed between NaCl and Fe on one side as an additional pressure standard. After drying a whole DAC with the sample in it in an oven, we loaded liquid H using a liquid hydrogen-introducing system at temperatures below 20 K (Chi et al., 2011; Tagawa et al., 2016).

After compression to 15–30 GPa, dhcp FeH was synthesized by laser heating to ~1000 K under hydrogen-saturated conditions in a DAC. High-temperature experiments above 60

GPa under such hydrogen-saturated conditions will form FeH_2 and FeH_3 from FeH and H_2 (Pépin et al., 2014). Therefore, after synthesizing FeH at such pressure range, we fully released pressure at liquid nitrogen temperature (~85 K) in an N_2 atmosphere, removed excess hydrogen from a sample chamber while maintaining FeH, and repressurized the sample to >5 GPa under cryogenic temperature. It is known that metastable FeH is quenchable to 1 bar at low temperatures and begins to decompose and release hydrogen above ~200 K (see Fig. 2 in Antonov et al., 2019). No excess hydrogen remained in the sample chamber, which is supported by the fact that neither FeH_2 nor FeH_3 was formed upon heating in their stability fields (Pépin et al., 2014). During recompression, the volume of the dhcp phase was obtained at 300 K each time with thermal annealing to ~1000–1400 K. We then heated the sample to >1500 K at ~40–60 GPa and observed a complete transformation from dhcp to fcc FeH (Isaev et al., 2007; Thompson et al., 2018; Kato et al., 2020) (Figure 2).

Structural determination and volume measurement were made on the basis of in-situ high *P-T* XRD spectra obtained at BL10XU, SPring-8 (Hirao et al., 2020). The incident X-ray beam was monochromatized to a wavelength of 0.41331–0.41463 Å (~30 keV) and focused to 6 μm in diameter. We collected diffraction data on a flat panel X-ray detector (PerkinElmer). The sample was heated from both sides with a couple of 100 W single-mode Yb fiber lasers. A laser beam was converted to one with a flat energy distribution by beam-shaping optics, and the laser-heated spot was 30–40 μm across. Sample temperature, T_{sample}, is an average for both sides of the sample. The temperature at each side is also averaged over 6–8 μm area at a laser-heated hot spot, which corresponds to the X-ray beam size. We consider the temperature uncertainty to be ±5% according to Mori et al. (2017). Pressure was determined from the unit-cell volume of NaCl (pressure medium) using its thermal EoS (Dorogokpets & Dewaele, 2007). We followed Campbell et al. (2009) to estimate the effective temperature of the pressure medium; $T_{NaCl} = \frac{3\times T_{sample}+300}{4} \pm \frac{T_{sample}-300}{4}$. Such pressure at high temperature has been validated by estimates using both NaCl and KCl pressure standards in run #3. KCl may give pressures more accurately in particular when a pressure marker plays also as a pressure medium and thus its temperature variation is relatively large, because the thermal expansivity of KCl is much smaller than that of NaCl. We found that the pressures from NaCl are almost identical with those calculated by using the EoS of KCl proposed by Tateno et al. (2019) (Figure S1 in the Supporting Information).

2.2. First-principles Calculations

We also performed first-principles calculations for fcc FeH in a way similar to that in Gomi et al. (2018). The Kohn-Sham equation was solved by the Korringa-Kohn-Rostoker (KKR) method (Akai, 1989). The Perdew-Burke-Ernzerhof type generalized gradient approximation was used for the exchange-correlation potential (Perdew et al., 1996). Relativistic effects were taken into account within the scalar relativistic approximation. The wavefunction was calculated up to $l = 2$, where l is angular momentum quantum number. The number of k-points was set to be 1240 in the irreducible Brillouin zone, which corresponds to 18 × 18 × 18 k-point mesh in the full Brillouin zone. The computational cell is an fcc Bravais lattice containing one FeH. The muffin-tin approximation was used. The muffin radii for the Fe site and the interstitial octahedral H site were set to be $r_{Fe} = 0.35355 \times a$ and $r_H = 0.14645 \times a$, respectively, where a is lattice parameter. The volume of the calculation cell ranged from 50 to 120 Bohr^3 with 2 Bohr^3 steps. FM, NM, and local moment disordered (LMD) states were calculated (see text in the Supporting Information, Figures S2a–c); the LMD state is a disordered binary alloy with up and down spin components that approximates the paramagnetic (PM) state above the Curie temperature within the coherent potential approximation (e.g., Akai & Dederichs, 1993; Gomi et al., 2018).

3. Results

The *P-V-T* data of fcc FeH were collected in a wide *P-T* range up to 146 GPa in *P* and 3720 K in *T* (Figure 1a, Dataset S1 in the Supporting Information). Melting was not observed even at such high temperatures, while Sakamaki et al. (2009) reported relatively low melting temperatures for FeH below 20 GPa. We employ volume data obtained only at high temperatures or at 300 K after heating, in order to avoid the effect of deviatoric stress on a sample. The fcc phase observed here was formed from dhcp FeH (Figure 2) and should be stoichiometric FeH because the volumes of both phases are on a single compression curve at 300 K before and after the transformation (Figure S3); note that the dhcp phase formed under hydrogen-saturated conditions is stoichiometric FeH in which H atoms fully occupy the octahedral sites (Antonov et al., 1998). The fcc phase being stoichiometric FeH in this study is also supported by the fact that its volume agrees with that formed in the presence of excess H_2 in Kato et al. (2020). The volume of dhcp FeH was measured in run #1 at 22–61 GPa (Dataset S1).

Our total energy calculations demonstrate that the FM state is stable for fcc FeH at ambient pressure and the FM-NM transition occurs at 47 GPa and 0 K (see text in the

Supporting Information, Figure S2b). The FM state changes to PM above the Curie temperature, which rapidly decreases with compression (Figure S2c). The local spin moment of the PM state will be quenched at the volume larger than that for FM (Figure S2a), indicating that the PM fcc FeH is also expected to lose its local spin moment at pressure lower than 47 GPa.

The present *P*-*V* data of fcc FeH obtained at 300 K are compared with the compression curves previously reported by experiments for the dhcp and fcc phases (Badding et al., 1991; Hirao et al., 2004; Narygina et al., 2011; Pépin et al., 2014; Kato et al., 2020) (Figure S3 in the Supporting Information). Deviations among these studies including the present one may be attributed to the difference in the magnetic state, resulting from different crystal structure, as well as thermal annealing during compression. The extrapolated compression curves reported by Hirao et al. (2004) and Narygina et al. (2011) disagree with ours because volumes were measured in limited pressure ranges in these two earlier experiments.

Here we obtain the room-temperature Vinet *P*-*V* EoS for the NM state by using the present 300 K data collected only above 41 GPa considering the pressure uncertainty in our first-principles calculations;

$$P = 3K_{0,300K}\left(\frac{V}{V_{0,300K}}\right)^{-2/3}\left[1-\left(\frac{V}{V_{0,300K}}\right)^{1/3}\right]\exp\left\{\frac{3}{2}(K'_{0,300K}-1)\left[1-\left(\frac{V}{V_{0,300K}}\right)^{1/3}\right]\right\} \quad (1)$$

High-temperature (>1600 K) FeH data were acquired for the NM state above 41 GPa in this study (Figure 1a). These data are fitted by the Mie-Grüneisen-Debye model (e.g., Dewaele et al., 2006);

$$P_{th}(V,T) = \frac{\gamma(V)}{V}\{E_{th}(T,V) - E_{th}(300K,V)\} \quad (2)$$

$$E_{th} = 9nk_{\mathrm{B}}\left(\frac{\Theta_D}{8} + T\left(\frac{T}{\Theta_D}\right)^3\int_0^{\Theta_D/T}\frac{x^3}{exp(x)-1}dx\right) \quad (3)$$

$$\Theta_D = \Theta_0 x^{-\gamma_\infty}\exp\left[\frac{\gamma_0-\gamma_\infty}{\beta}(1-x^\beta)\right] \quad (4)$$

$$\beta = \frac{\gamma_0}{\gamma_0-\gamma_\infty} \quad (5a)$$

$$\gamma(V) = \gamma_\infty + (\gamma_0-\gamma_\infty)\,x^\beta \quad (5b)$$

where E_{th} is thermal energy, γ is Grüneisen parameter (subscript 0 and ∞ denote values at ambient and infinitely compressed conditions, respectively), Θ_D is Debye temperature, n is the number of atoms per formula unit (n = 2 for FeH), k_B is Boltzmann's constant in GPa·Å^3·K^{-1} unit, and β is a fitted parameter. Θ_D is also formulated from the Debye sound velocity as;

$$\Theta_D = \frac{h}{2\pi\, k_B}\left(\frac{6\pi^2 N}{V}\right)^{\frac{1}{3}} v_D \tag{6}$$

where h is Planck's constant and v_D is bulk sound speed. We estimated Θ_0, γ_0, and γ_∞ to be consistent with both our P-V-T data and v_D reported by Thompson et al. (2018) from NRIXS measurements above 41 GPa. These fittings provide V_0 = 13.45(15) Å^3 for a formula unit, K_0 = 183(20) GPa, K' = 3.84(37), Θ_0 = 758 K (fixed), n = 2, γ_0 = 0.738 (40), and γ_∞ = 0.547(83). These parameters are compared with those for fcc pure Fe (Tsujino et al., 2013) and for dhcp FeH based on data collected below 20 GPa (Sakamaki et al., 2009) in Table S1. The present EoS for the NM state predicts smaller volumes than observed by Sakamaki et al. (2009) for the FM and possibly PM (with local spin moment) states at <21 GPa and high temperatures to 1573 K (Figure 1b).

4. Discussion

4.1. ΔV_H at High P and T

We obtain ΔV_H from the difference in volume between FeH and Fe. Here we employ the EoSs of fcc and hcp Fe for the NM state reported by Dorogokupets et al. (2017), in which pressure was calibrated to be consistent with the NaCl scale by Dorogokpets & Dewaele (2007) that is employed in this study. The room-temperature ΔV_H for both fcc and dhcp FeH is shown as a function of pressure in Figure 3a. The volume of dhcp FeH was obtained in run #1 between 22 and 57 GPa, and ΔV_{H_dhcp} is calculated by using the volume of hcp Fe which is similar in structure to dhcp. ΔV_{H_dhcp} is larger than ΔV_{H_fcc} for the fcc phase at relatively low pressures, which is also evident from neutron diffraction experiments at <5 GPa (Antonov et al., 1998; Machida et al., 2014; Ikuta et al., 2019). Nevertheless, ΔV_{H_dhcp} decreases more rapidly than ΔV_{H_fcc} with compression, and both become similar above 45 GPa. Such behavior of ΔV_{H_dhcp} is likely attributed to the FM to NM transition in dhcp FeH (Ying et al., 2020). Also, ΔV_{H_fcc} data below 40 GPa including neutron diffraction data at 4.2 GPa are for the FM and possibly PM (with local spin moment) states and larger than that for its NM state (Figure 3a). It is noted that once Fe loses its local spin moment, ΔV_{H_dhcp} and ΔV_{H_fcc} are similar to each other, suggesting that ΔV_H for the NM state does not depend on the crystal structure and is applicable to hcp

Fe-H alloys.

The present experiments give not only the pressure effect but also the temperature dependence of $\Delta V_H(P, T)$ for the NM state (Figure 3b), which has not been demonstrated previously except for the recent calculations by Wang et al. (2021) performed only at 360 GPa and 2000–6500 K (Figure 3c). As demonstrated in these figures, ΔV_H diminishes with increasing temperature likely because the interstitial sites for H around Fe atoms expand at high temperature; the ΔV_H decreases by about 10% at 2000 K in a wide pressure range and by 16–20% at inner core boundary (ICB) conditions of 330 GPa and 5400–6000 K.

Fitting Vinet EoS (Eq. 1) to ΔV_{H_fcc} data at 300 K for NM FeH gives V_0 = 2.097(1) Å^3, K_0 = 301.2(9) GPa, and K' = 1.404(6). And, the temperature effect can be approximated as; $\Delta V_{H\_fcc}(P, T) = -0.00241(1) \times P - 1.338(13) \times 10^{-4} \times T + 2.724(46) \times 10^{-7} \times P \times T + 1.872(3)$ (Figure 3b). This equation predicts ΔV_H that deviates by less than 0.1 Å from our experimental data at >60 GPa and 300–6600 K.

At 0–300 K, both ΔV_{H_dhcp} and ΔV_{H_fcc} observed here are remarkably smaller than the volume of metallic hydrogen, $\Delta V_{metal\text{-}H}$ (Figure 3a), which was calculated considering a close-packed structure and vibrational contributions by Chakravarty et al. (1981). The $\Delta V_{metal\text{-}H}$ was originally employed by Fukai (1992) and has been used to calculate H concentration in Fe-H alloys (e.g., Shibazaki et al., 2011; Terasaki et al., 2012). However, they were always underestimated by several tens % since $\Delta V_{metal\text{-}H}$ is substantially larger than ΔV_H in FeH. In contrast, the ΔV_{H_fcc} at room temperature is approximately consistent with that previously calculated at 0 K by Caracas (2015). When our ΔV_{H_fcc} is extrapolated to high P-T conditions for the Earth's inner core (330–364 GPa, >4800 K), it is broadly consistent with ΔV_{H_hcp} obtained for hcp $Fe_{60}Si_4H_8$ by first-principles calculations (Wang et al., 2021), although their calculations for $Fe_{64}H_4$ gave smaller values (Figure 3c).

4.2. Implications for Hydrogen in Earth's Inner Core

Hydrogen can be an important light impurity element in the Earth's outer core to explain its density and seismic velocity (Umemoto & Hirose, 2015, 2020). Previous multi-anvil experiments performed at 15–20 GPa demonstrated the solid-Fe/liquid-Fe partition coefficient of H, D_H(solid/liquid) to be ~0.7 by weight (Imai, 2013), indicating that hydrogen could be a major light element in the solid inner core as well. Indeed, the recent calculations by Wang et al. (2021) demonstrated that the inner core may include up to 0.23 wt% H together with Si, depending on its temperature.

ΔV_H (P, T) obtained above constrains H concentration in the inner core. If hydrogen is a sole light element, the inner core density is explained with 0.8–0.9 wt% H (0.78–0.85 wt% H at the ICB) considering its temperatures to be 4800–6600 K (Figure 4). We note that such estimate of the H content is almost independent on temperature, because the higher the inner core temperature is, the smaller the density deficit with respect to pure Fe is, but ΔV_H also becomes smaller (Figure 3c). It is not the case for silicon nor sulfur, another plausible light elements in the inner core. With the thermal EoSs of hcp Fe-9wt%Si alloy (Fischer et al., 2014) and Fe (Dorogokupets et al., 2017), the amount of Si required to explain the inner core density deficit as a single light element is estimated to be 4.1 wt% at the ICB pressure of 330 GPa and 4800 K, which decreases to 3.1 wt% with increasing temperature to 6600 K (Figure 4). Also, the experiments performed by Sakai et al. (2012) on an Fe-Ni-S alloy demonstrated that 5.3 to 3.6 wt% S explains the density at the inner core side of the ICB when the effect of nickel is not considered, depending on its temperature ranging from 4800 to 6600 K.

The Earth's inner core should be an Fe-H-Si-S(-Ni) alloy with least amounts of C and O because their solid-Fe/liquid-Fe partition coefficients are limited to 0 to 0.1 (Hasegawa et al., 2021; Li et al., 2019; Alfè et al., 2002; Ozawa et al., 2010). If the excess volume of mixing is negligible, the inner core composition may be represented by a mixture among Fe-0.85 wt% H, Fe-4.1 wt% Si, and Fe-5.3 wt% S when the ICB temperature is 4800 K. The possible ranges of the Fe-H-Si-S inner core composition are illustrated in Figure 4, depending on the ICB temperature ranging from 4800 to 6600 K. Furthermore, such possible ranges of the inner core composition can constrain the possible liquid outer core composition, once the partitioning of light elements between the outer and inner core is better understood including their interactions (e.g., Tateno et al., 2018; Tao and Fei, 2021; Hirose et al., 2021).

5. Conclusions

We constructed the high-temperature EoS of fcc FeH in the NM state based on its volume measurements of fcc FeH were carried out to 142 GPa and 3660 K in a laser-heated DAC, in which we avoided the formation of FeH_2 and FeH_3 by releasing excess H_2 from a sample chamber after the synthesis of stoichiometric FeH. According to our first-principles calculations, we employed data only above 41 GPa that represent the NM state. The EoS of FeH provides ΔV_H (P, T), the volume increase per H atom, for Fe-H alloys as functions of P and T, which we found does not depend on crystal structures at NM conditions. Such ΔV_H (P, T) is remarkably smaller than the volume of metallic H at

equivalent conditions and will be useful for *in-situ* quantification of H contents in Fe-H alloys under *P-T*. When extrapolated to inner core conditions, our ΔV_H (*P*, *T*) is in broad agreement with that by recent theoretical predictions (Wang et al., 2021). It gives the maximum H content in the inner core to be 0.8–0.9 wt%, which is almost independent of temperature because the higher the inner core temperature is, the smaller the density deficit is, but ΔV_H (*P*, *T*) also decreases. We also estimated the possible compositional range of the Fe-H-Si-S inner core.

Data Availability Statement

Datasets for this research are found in Dataset S1 available online (from https://doi.org/10.5281/zenodo.5513718).

Acknowledgments

Discussion with G. Helffrich on the magnetic state of FeH was valuable. We thank S. Tateno and K. Ohta for their support in our experiment. Synchrotron XRD measurements were made at BL10XU, SPring-8 (proposals no. 2018B0072, 2019A0072, and 2019B0072). This work was supported by the JSPS grants.

References

Akai, H. (1989). Fast Korringa-Kohn-Rostoker coherent potential approximation and its application to FCC Ni-Fe systems. *Journal of Physics: Condensed Matter*, *1*(43), 8045–8064. https://doi.org/10.1088/0953-8984/1/43/006

Akai, H., & Dederichs, P. H. (1993). Local moment disorder in ferromagnetic alloys. *Physical Review B*, *47*(14), 8739–8747. https://doi.org/10.1103/PhysRevB.47.8739

Alfé, D., Gillan, M. J., & Price, G. D. (2002). Composition and temperature of the earth's core constrained by combining ab initio calculations and seismic data. *Earth and Planetary Science Letters*, *195*(1–2), 91–98. https://doi.org/10.1016/S0012-821X(01)00568-4

Antonov, V., Cornell, K., Fedotov, V., Kolesnikov, A., Ponyatovsky, E., Shiryaev, V., & Wipf, H. (1998). Neutron diffraction investigation of the dhcp and hcp iron hydrides and deuterides. *Journal of Alloys and Compounds*, *264*(1–2), 214–222. https://doi.org/10.1016/S0925-8388(97)00298-3

Antonov, V. E., Gurev, V. M., Kulakov, V. I., Kuzovnikov, M. A., Sholin, I. A., & Zuykova, V. Y. (2019). Solubility of deuterium and hydrogen in fcc iron at high pressures and temperatures. *Physical Review Materials*, *3*(11), 113604.

https://doi.org/10.1103/PhysRevMaterials.3.113604

Badding, J. V., Hemley, R. J., & Mao, H. K. (1991). High-pressure chemistry of hydrogen in metals: in situ study of iron hydride. *Science*, *253*(5018), 421–424. https://doi.org/10.1126/science.253.5018.421

Campbell, A. J., Danielson, L., Righter, K., Seagle, C. T., Wang, Y., & Prakapenka, V. B. (2009). High pressure effects on the iron-iron oxide and nickel-nickel oxide oxygen fugacity buffers. *Earth and Planetary Science Letters*, *286*(3–4), 556–564. https://doi.org/10.1016/j.epsl.2009.07.022

Caracas, R. (2015). The influence of hydrogen on the seismic properties of solid iron. *Geophysical Research Letters*, *42*(10), 3780–3785. https://doi.org/10.1002/2015GL063478

Chakravarty, S., Rose, J. H., Wood, D., & Ashcroft, N. W. (1981). Theory of dense hydrogen. *Physical Review B*, *24*(4), 1624–1635. https://doi.org/10.1103/PhysRevB.24.1624

Chi, Z., Nguyen, H., Matsuoka, T., Kagayama, T., Hirao, N., Ohishi, Y., & Shimizu, K. (2011). Cryogenic implementation of charging diamond anvil cells with H_2 and D_2. *The Review of Scientific Instruments*, *82*(10), 105109. https://doi.org/10.1063/1.3652981

Dewaele, A., Loubeyre, P., Occelli, F., Mezouar, M., Dorogokupets, P. I., & Torrent, M. (2006). Quasihydrostatic equation of state of iron above 2 Mbar. *Physical Review Letters*, *97*(21), 215504. https://doi.org/10.1103/PhysRevLett.97.215504

Dorogokupets, P. I., & Dewaele, A. (2007). Equations of state of MgO, Au, Pt, NaCl-B1, and NaCl-B2: internally consistent high-temperature pressure scales. *High Pressure Research*, *27*(4), 431–446. https://doi.org/10.1080/08957950701659700

Dorogokupets, P. I., Dymshits, A. M., Litasov, K. D., & Sokolova, T. S. (2017). Thermodynamics and equations of state of iron to 350 GPa and 6000 K. *Scientific Reports*, *7*(1), 41863. https://doi.org/10.1038/srep41863

Fischer, R. A., Campbell, A. J., Caracas, R., Reaman, D. M., Heinz, D. L., Dera, P., & Prakapenka, V. B. (2014). Equations of state in the Fe-FeSi system at high pressures and temperatures. *Journal of Geophysical Research: Solid Earth*, *119*(4), 2810–2827. https://doi.org/10.1002/2013JB010898

Fukai, Y., & Suzuki, T. (1986). Iron–water reaction under high pressure and its implication in the evolution of the Earth. *J. Geophys. Res.*, *91*(B9), 9222–9230. https://doi.org/10.1029/JB091iB09p09222

Fukai, Y. (1992). Some properties of the Fe-H system at high pressures and temperatures, and their implications for the Earth's core. In Y. Syono, M.H. Manghnani (Eds.), *High-*

pressure research: applications to Earth and planetary sciences (Vol. 67, pp. 373–385). https://doi.org/10.1029/GM067p0373

Gomi, H., Fei, Y., & Yoshino, T. (2018). The effects of ferromagnetism and interstitial hydrogen on the equation of states of hcp and dhcp FeH*x*: implications for the Earth's inner core age. *American Mineralogist*, *103*(8), 1271–1281. https://doi.org/10.2138/am-2018-6295

Hasegawa, M., Hirose, K., Oka, K., & Ohishi, Y. (2021). Liquidus phase relations and solid-liquid partitioning in the Fe-Si-C system under core pressures. *Geophysical Research Letters*, *48*(13), e2021GL092681. https://doi.org/10.1029/2021gl092681

Hirao, N., Kawaguchi, S. I., Hirose, K., Shimizu, K., Ohtani, E., & Ohishi, Y. (2020). New developments in high-pressure X-ray diffraction beamline for diamond anvil cell at SPring-8. *Matter and Radiation at Extremes*, *5*(1), 1–10. https://doi.org/10.1063/1.5126038

Hirao, N., Kondo, T., Ohtani, E., Takemura, K., & Kikegawa, T. (2004). Compression of iron hydride to 80 GPa and hydrogen in the Earth's inner core. *Geophysical Research Letters*, *31*(6), L06616. https://doi.org/10.1029/2003GL019380

Hirose, K., Wood, B., & Vočadlo, L. (2021). Light elements in the Earth's core. *Nature Reviews Earth & Environment*, *2*, 645–658. https://doi.org/10.1038/s43017-021-00203-6

Ikoma, M., & Genda, H. (2006). Constraints on the mass of a habitable planet with water of nebular origin. *The Astrophysical Journal*, *648*(1), 696–706. https://doi.org/10.1086/505780

Ikuta, D., Ohtani, E., Sano-Furukawa, A., Shibazaki, Y., Terasaki, H., Yuan, L., & Hattori, T. (2019). Interstitial hydrogen atoms in face-centered cubic iron in the Earth's core. *Scientific Reports*, *9*(1), 7108. https://doi.org/10.1038/s41598-019-43601-z

Imai, T. (2013). *Hydrogen partitioning between iron and silicate and melting phase relation in the system Fe-FeH*, (Doctoral dissertation). Tokyo, Japan: Tokyo Institute of Technology.

Isaev, E. I., Skorodumova, N. V, Ahuja, R., Vekilov, Y. K., & Johansson, B. (2007). Dynamical stability of Fe-H in the Earth's mantle and core regions. *Proceedings of the National Academy of Sciences of the United States of America*, *104*(22), 9168–9171. https://doi.org/10.1073/pnas.0609701104

Kato, C., Umemoto, K., Ohta, K., Tagawa, S., Hirose, K., & Ohishi, Y. (2020). Stability of fcc phase FeH to 137 GPa. *American Mineralogist*, *105*(6), 917–921. https://doi.org/10.2138/am-2020-7153

Li, Y., Vočadlo, L., Sun, T., & Brodholt, J. P. (2020). The Earth's core as a reservoir of

water. *Nature Geoscience*, *13*(6), 453–458. https://doi.org/10.1038/s41561-020-0578-1

Li, Y., Vočadlo, L., Alfè, D., & Brodholt, J. (2019). Carbon partitioning between the Earth's inner and outer core. *Journal of Geophysical Research: Solid Earth*, *124*(12), 12812–12824. https://doi.org/10.1029/2019JB018789

Machida, A., Saitoh, H., Sugimoto, H., Hattori, T., Sano-Furukawa, A., Endo, N., et al. (2014). Site occupancy of interstitial deuterium atoms in face-centred cubic iron. *Nature Communications*, *5*(1), 5063. https://doi.org/10.1038/ncomms6063

Machida, A., Saitoh, H., Hattori, T., Sano-Furukawa, A., Funakoshi, K., Sato, T., et al. (2019). Hexagonal close-packed iron hydride behind the conventional phase diagram. *Scientific Reports*, *9*(1), 12290. https://doi.org/10.1038/s41598-019-48817-7

Mori, Y., Ozawa, H., Hirose, K., Sinmyo, R., Tateno, S., Morard, G., & Ohishi, Y. (2017). Melting experiments on Fe–Fe_3S system to 254 GPa. *Earth and Planetary Science Letters*, *464*, 135–141. https://doi.org/10.1016/j.epsl.2017.02.021

Narygina, O., Dubrovinsky, L. S., McCammon, C. A., Kurnosov, A., Kantor, I. Y., Prakapenka, V. B., & Dubrovinskaia, N. A. (2011). X-ray diffraction and Mössbauer spectroscopy study of fcc iron hydride FeH at high pressures and implications for the composition of the Earth's core. *Earth and Planetary Science Letters*, *307*(3–4), 409–414. https://doi.org/10.1016/j.epsl.2011.05.015

Ohta, K., Ichimaru, K., Einaga, M., Kawaguchi, S., Shimizu, K., Matsuoka, T., et al. (2015). Phase boundary of hot dense fluid hydrogen. *Scientific Reports*, *5*(1), 16560. https://doi.org/10.1038/srep16560

Olson, P. L., & Sharp, Z. D. (2019). Nebular atmosphere to magma ocean: a model for volatile capture during Earth accretion. *Physics of the Earth and Planetary Interiors*, *294*, 106294. https://doi.org/10.1016/j.pepi.2019.106294

Ozawa, H., Hirose, K., Tateno, S., Sata, N., & Ohishi, Y. (2010). Phase transition boundary between B1 and B8 structures of FeO up to 210 GPa. *Physics of the Earth and Planetary Interiors*, *179*(3–4), 157–163. https://doi.org/10.1016/j.pepi.2009.11.005

Pépin, C. M., Dewaele, A., Geneste, G., Loubeyre, P., & Mezouar, M. (2014). New iron hydrides under high pressure. *Physical Review Letters*, *113*(26), 265504. https://doi.org/10.1103/PhysRevLett.113.265504

Perdew, J. P., Burke, K., & Ernzerhof, M. (1996). Generalized gradient approximation made simple. *Physical Review Letters*, *77*(18), 3865–3868. https://doi.org/10.1103/PhysRevLett.77.3865

Raymond, S. N., & Morbidelli, A (2020). Planet formation: key mechanisms and global

models. Preprint at https://arxiv.org/pdf/2002.05756.pdf

Sakai, T., Ohtani, E., Kamada, S., Terasaki, H., & Hirao, N. (2012). Compression of $Fe_{88.1}Ni_{9.1}S_{2.8}$ alloy up to the pressure of Earth's inner core. *Journal of Geophysical Research: Solid Earth*, *117*, B02210. https://doi.org/10.1029/2011JB008745

Sakamaki, K., Takahashi, E., Nakajima, Y., Nishihara, Y., Funakoshi, K., Suzuki, T., & Fukai, Y. (2009). Melting phase relation of FeH*x* up to 20 GPa: implication for the temperature of the Earth's core. *Physics of the Earth and Planetary Interiors*, *174*(1–4), 192–201. https://doi.org/10.1016/j.pepi.2008.05.017

Shibazaki, Y., Ohtani, E., Terasaki, H., Tateyama, R., Sakamaki, T., Tsuchiya, T., & Funakoshi, K. (2011). Effect of hydrogen on the melting temperature of FeS at high pressure: Implications for the core of Ganymede. *Earth and Planetary Science Letters*, *301*(1–2), 153–158. https://doi.org/10.1016/j.epsl.2010.10.033

Stähler, S. C., Khan, A., Banerdt, W. B., Lognonné, P., Giardini, D., Ceylan, S., et al. (2021). Seismic detection of the martian core. *Science*, *373*(6553), 443–448. https://doi.org/10.1126/science.abi7730

Tagawa, S., Ohta, K., Hirose, K., Kato, C., & Ohishi, Y. (2016). Compression of Fe-Si-H alloys to core pressures. *Geophysical Research Letters*, *43*(8), 3686–3692. https://doi.org/10.1002/2016GL068848

Tagawa, S., Sakamoto, N., Hirose, K., Yokoo, S., Hernlund, J., Ohishi, Y., & Yurimoto, H. (2021). Experimental evidence for hydrogen incorporation into Earth's core. *Nature Communications*, *12*(1), 2588. https://doi.org/10.1038/s41467-021-22035-0

Tao, R., & Fei, Y. (2021). High-pressure experimental constraints of partitioning behavior of Si and S at the Mercury's inner core boundary. *Earth and Planetary Science Letters*, *562*, 116849. https://doi.org/10.1016/j.epsl.2021.116849

Tateno, S., Komabayashi, T., Hirose, K., Hirao, N., & Ohishi, Y. (2019). Static compression of B2 KCl to 230 GPa and its P-V-T equation of state. *American Mineralogist*, *104*(5), 718–723. https://doi.org/10.2138/am-2019-6779

Terasaki, H., Ohtani, E., Sakai, T., Kamada, S., Asanuma, H., Shibazaki, Y., et al. (2012). Stability of Fe-Ni hydride after the reaction between Fe-Ni alloy and hydrous phase (δ-AlOOH) up to 1.2Mbar: possibility of H contribution to the core density deficit. *Physics of the Earth and Planetary Interiors*, *194–195*, 18–24. https://doi.org/10.1016/j.pepi.2012.01.002

Thompson, E. C., Davis, A. H., Bi, W., Zhao, J., Alp, E. E., Zhang, D., et al. (2018). High-pressure geophysical properties of fcc phase FeH*x*. *Geochemistry, Geophysics, Geosystems*, *19*(1), 305–314. https://doi.org/10.1002/2017GC007168

Tsujino, N., Nishihara, Y., Nakajima, Y., Takahashi, E., Funakoshi, K., & Higo, Y. (2013).

Equation of state of γ-Fe: reference density for planetary cores. *Earth and Planetary Science Letters*, *375*, 244–253. https://doi.org/10.1016/j.epsl.2013.05.040

Umemoto, K., & Hirose, K. (2015). Liquid iron-hydrogen alloys at outer core conditions by first-principles calculations. *Geophysical Research Letters*, *42*(18), 7513–7520. https://doi.org/10.1002/2015GL065899

Umemoto, K., & Hirose, K. (2020). Chemical compositions of the outer core examined by first principles calculations. *Earth and Planetary Science Letters*, *531*, 116009. https://doi.org/10.1016/j.epsl.2019.116009

Wang, W., Li, Y., Brodholt, J. P., Vočadlo, L., Walter, M. J., & Wu, Z. (2021). Strong shear softening induced by superionic hydrogen in Earth's inner core. *Earth and Planetary Science Letters*, *568*, 117014. https://doi.org/10.1016/j.epsl.2021.117014

Ying, J., Zhao, J., Bi, W., Alp, E. E., Xiao, Y., Chow, P., et al. (2020). Magnetic phase diagram of ε'-FeH. *Physical Review B*, *101*(2), 020405. https://doi.org/10.1103/PhysRevB.101.020405

Yuan, L., & Steinle-Neumann, G. (2020). Strong sequestration of hydrogen into the Earth's core during planetary differentiation. *Geophysical Research Letters*, *47*(15), e2020GL088303. https://doi.org/10.1029/2020GL088303

References From the Supporting Information

Sato, K., Dederics, P. H., & Katayama-Yoshida, H. (2003). Curie temperatures of III–V diluted magnetic semiconductors calculated from first principles. *EPL*, *61*(3), 403–408. https://doi.org/10.1209/epl/i2003-00191-8

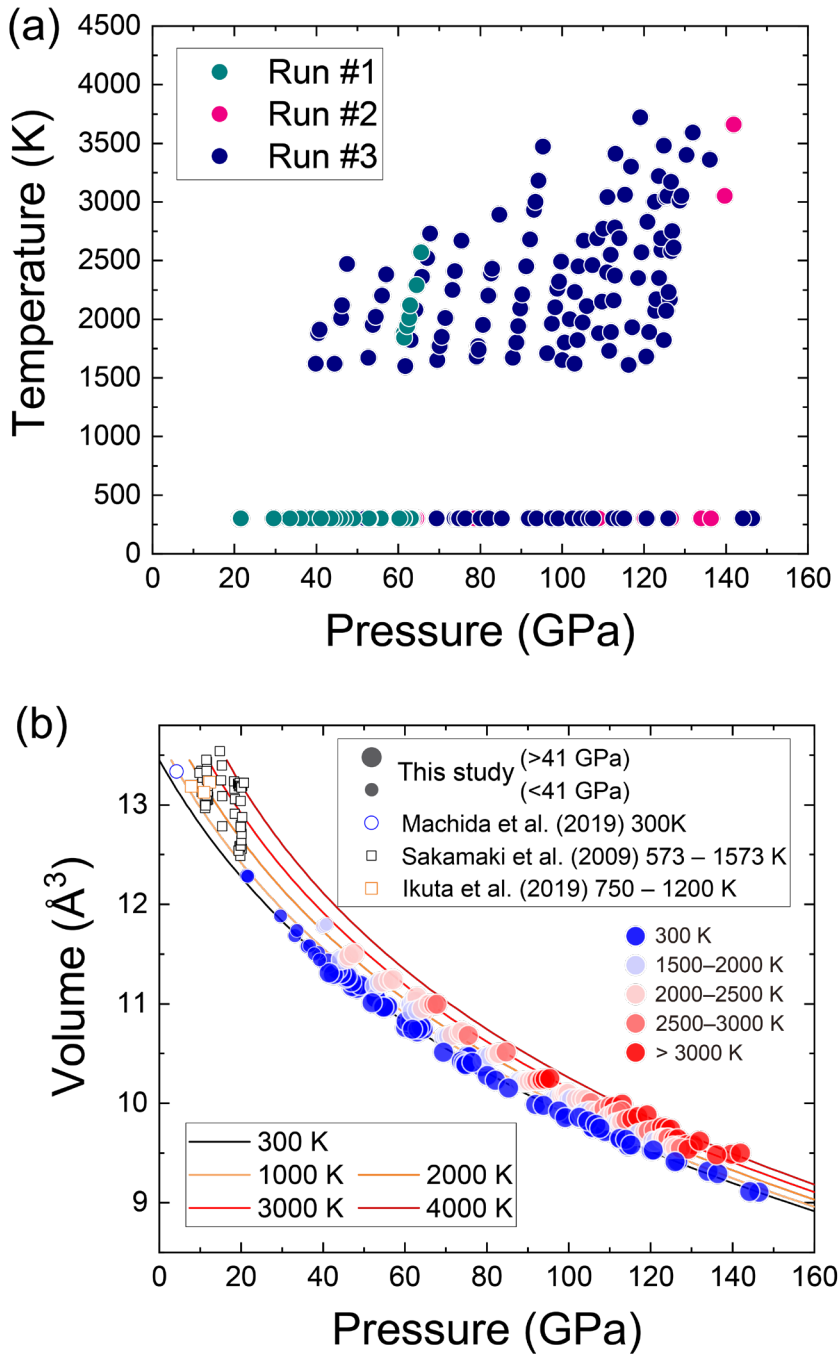

Figure 1. (a) *P-T* conditions for measuring the volume of FeH in runs #1–3. (b) *P-V* data for fcc FeH at 300 K and high temperatures. Closed large circles, this study; small open circle, Machida et al. (2019) at 300 K; black squares, Sakamaki et al. (2009) at 573–1573 K; yellow squares, Ikuta et al. (2019) at 750–1200 K. Errors in pressure and volume are presented in Dataset S1. Isothermal compression curves are for the NM state stable above ~40 GPa. They deviate from previous low-pressure measurements on the FM and PM (with local spin moment) states.

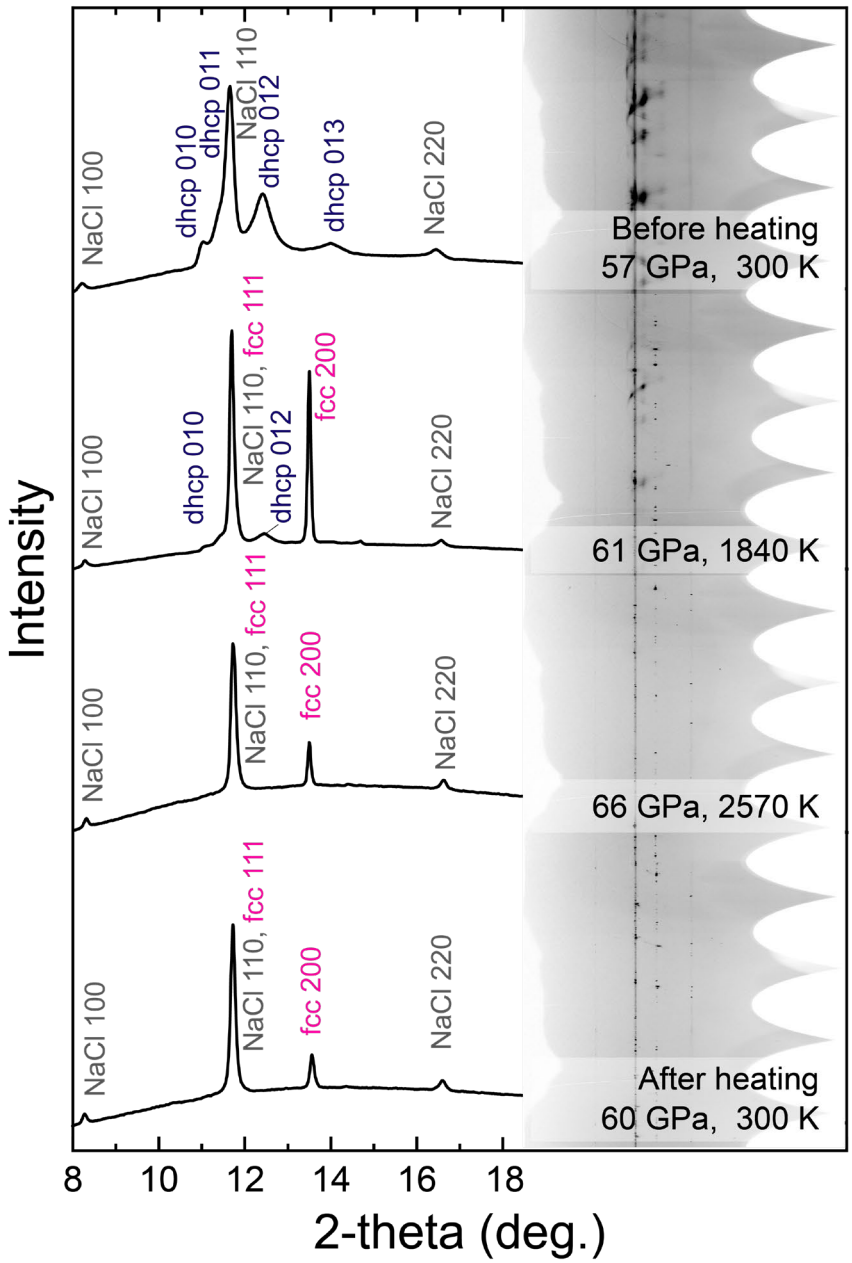

Figure 2. XRD data collected in run #1 before heating for dhcp FeH and during/after heating for the fcc phase.

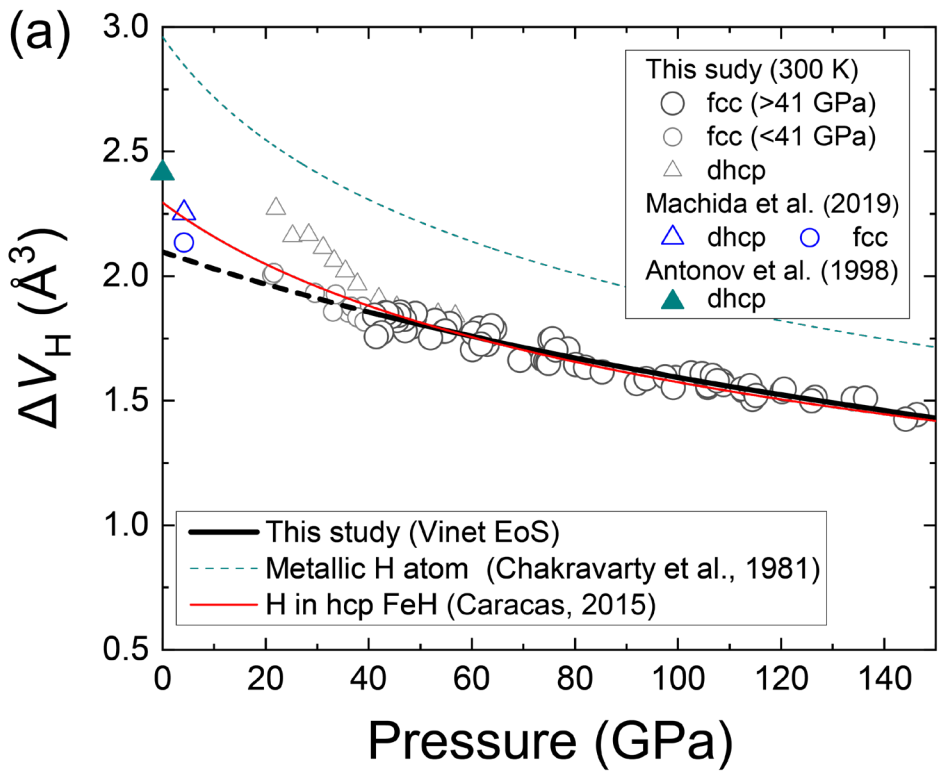
(a)
This sudy (300 K)
fcc (>41 GPa)
fcc (<41 GPa)
dhcp
Machida et al. (2019)
dhcp
fcc
Antonov et al. (1998)
dhcp
This study (Vinet EoS)
Metallic H atom (Chakravarty et al., 1981)
H in hcp FeH (Caracas, 2015)
ΔV_H (Å^3)
Pressure (GPa)

506

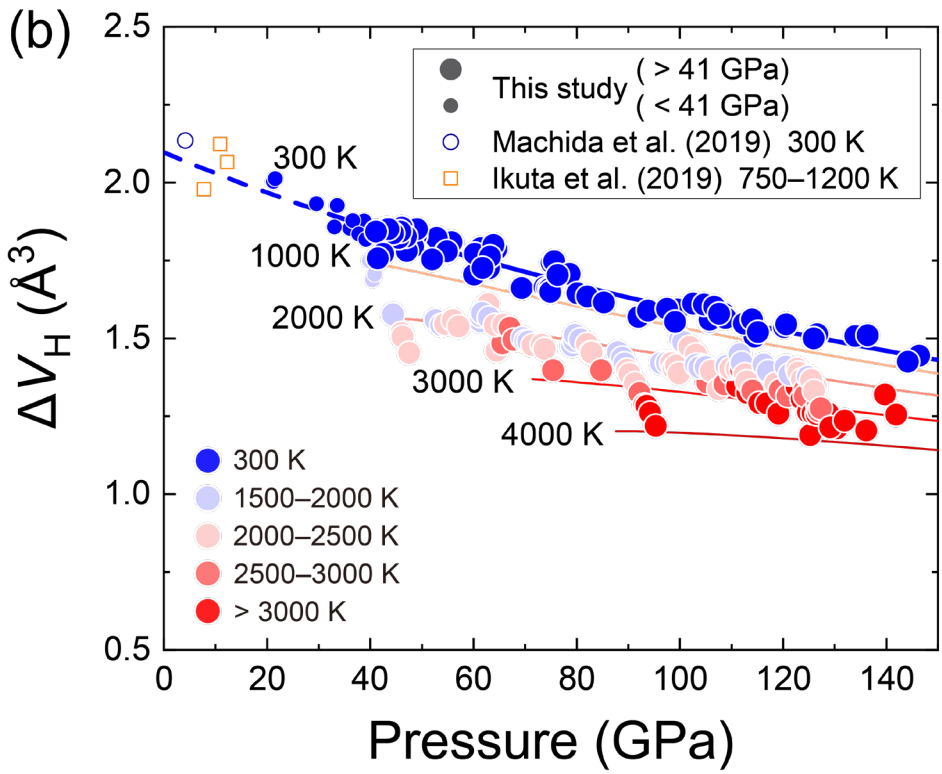
(b)
This study (> 41 GPa)
(< 41 GPa)
Machida et al. (2019) 300 K
Ikuta et al. (2019) 750–1200 K
300 K
1000 K
2000 K
3000 K
4000 K
300 K
1500–2000 K
2000–2500 K
2500–3000 K
> 3000 K
ΔV_H (Å^3)
Pressure (GPa)

507

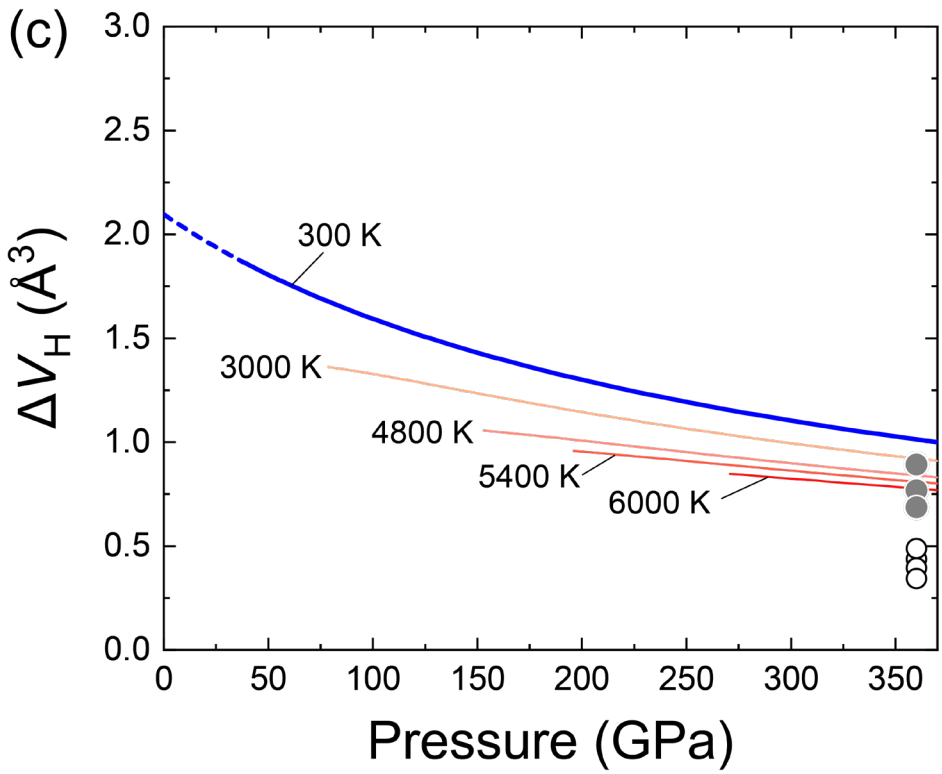

Figure 3. (a) ΔV_H at 300 K and high pressures obtained for fcc (circles) and dhcp (triangles) FeH (black solid line). Data by neutron diffraction measurements at low pressures are from Machida et al. (2019) (blue) and Antonov et al. (1998) (green). Large and small symbols represent the data for NM and FM (or PM with local spin moment) states, respectively. They are much smaller than the calculated volume of metallic H (Chakravarty et al., 1981) (green broken line), which was employed by Fukai (1992) to estimate H concentration in Fe-H alloys. The present data for NM fcc FeH is consistent with the ΔV_H calculated for hcp FeH at 0 K by Caracas (2015) (red line). (b) Changes in ΔV_H for NM (large circles) and FM (or PM with local spin moment) (small circles and squares) fcc FeH at high pressures with increasing temperature. Neutron diffraction data (open symbols) are given for 300 K (Machida et al., 2019) and 750–1200 K (Ikuta et al., 2019). Colored curves indicate the effect of temperature from 300 to 4000 K. (c) ΔV_H extrapolated to inner core *P-T* (colored curves). Data for hcp $Fe_{60}Si_4H_8$ (gray circles) and $Fe_{64}H_4$ (open circles) by first-principles calculations (Wang et al., 2021) are also plotted.

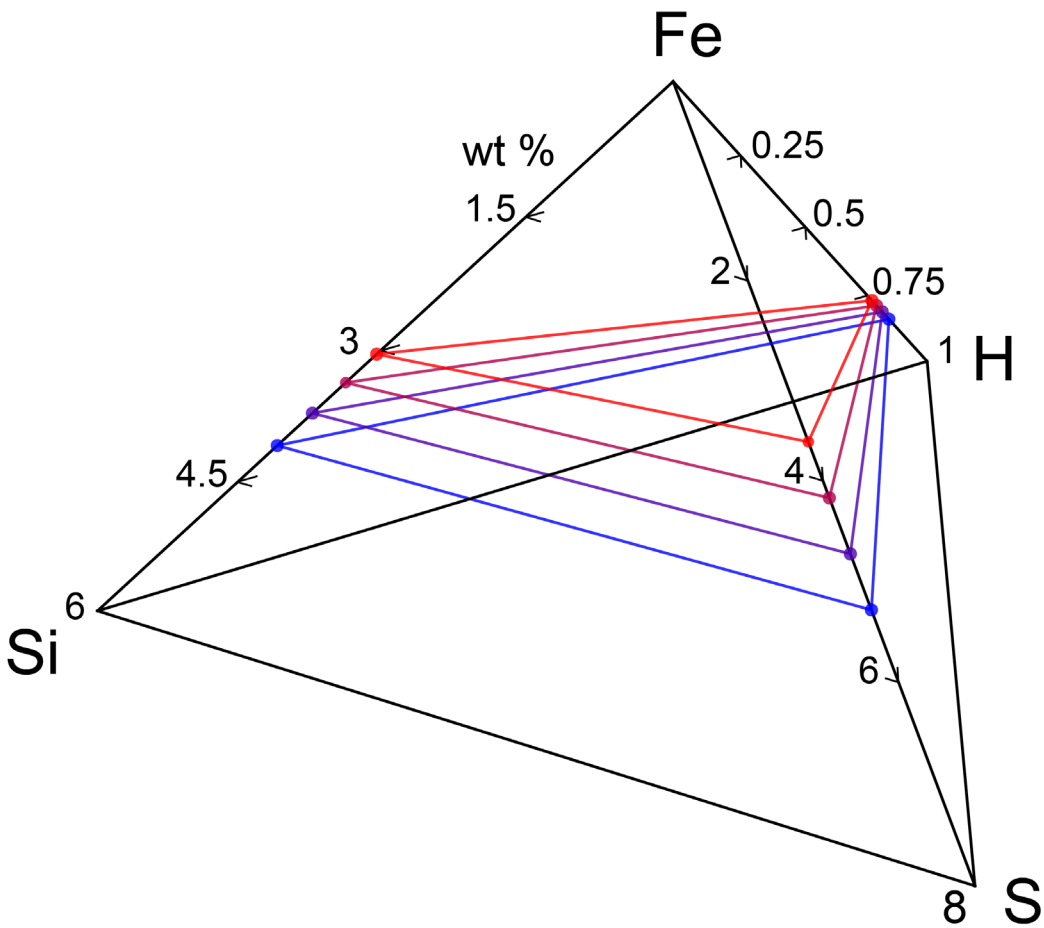

Figure 4. Possible ranges of the Fe-H-Si-S inner composition illustrated by each triangle plane depending on ICB temperature (blue, 4800 K; purple, 5400 K; magenta, 6000 K; red, 6600 K).

Geophysical Research Letters

Supporting Information for

High-Temperature Equation of State of FeH: Implications for Hydrogen in Earth's Inner Core

Shoh Tagawa[1,2], Hitoshi Gomi[1], Kei Hirose[1,2], and Yasuo Ohishi[3]

[1]Earth-Life Science Institute, Tokyo Institute of Technology, Tokyo, Japan

[2]Department of Earth and Planetary Science, The University of Tokyo, Tokyo, Japan

[3]Japan Synchrotron Radiation Research Institute, SPring-8, Hyogo, Japan

Contents of this file

Text

Table S1

Figures S1–S3

Additional Supporting Information

Dataset S1

Magnetic States of fcc FeH at High Pressure

Our first-principles calculations of fcc FeH show the local spin moments (within the muffin-tin sphere of the Fe site) of FM and LMD states as a function of volume at $T = 0$ K (Figure S2a). The local spin moment in the FM state is present down to 76 Bohr^3 (11.26 Å^3) and disappears abruptly below 74 Bohr^3 (10.97 Å^3). On the other hand, that in the LMD state decreases slowly with decreasing volume and is completely quenched at 78 Bohr^3 (11.56 Å^3). The total energy calculations demonstrate that the FM state is stable at ambient pressure (Figure S2b).

Their total energies of FM, LMD, and NM states were fitted to the Vinet EoS;

$$E(V) = \frac{2K_0V_0}{(K_0'-1)^2}\left\{2 - \left[5 + 3\left(\frac{V}{V_0}\right)^{\frac{1}{3}}(K_0'-1) - 3K_0'\right]\exp\left[-\frac{3}{2}(K_0'-1)\left[\left(\frac{V}{V_0}\right)^{\frac{1}{3}} - 1\right]\right]\right\} + E_0, \quad \text{(S1)}$$

where E is total energy, and K and K' are bulk modulus and its pressure derivative, respectively. The subscript 0 denotes the value at zero pressure. For the FM state, fitting was made for the volume range of 76–120 Bohr^3, where the finite local spin moment exists. Similarly, the LMD state was fitted in the range of 80–120 Bohr^3. The obtained fitting parameters sets are V_0 = 13.55 Å^3, K_0 = 186.10 GPa, K_0' = 4.54 for the FM state, V_0 = 13.22 Å^3, K_0 = 167.08 GPa, K_0' = 4.04 for the LMD state, and V_0 = 12.51 Å^3, K_0 = 261.71 GPa, K_0' = 4.08 for the NM state. With these parameters sets, we calculated pressure from the P-V relation of the same form as Eq. 1 in the main text. The FM-NM transition pressure is found to be 47 GPa at 0 K from the comparison of enthalpy ($E + PV$). The FM-PM transition temperature (Curie temperature) is also estimated by comparing the energies of the FM and LMD states as (Sato et al., 2003);

$$T_C = \frac{2}{3k_B}(E_{LMD} - E_{FM}), \quad \text{(S2)}$$

where T_C is the Curie temperature, k_B is Boltzmann's constant, and E_{LMD} and E_{FM} are the total energies of the LMD and FM states, respectively (Figure S2c). The obtained Curie temperature is about 1100 K at ambient pressure, which is comparable to the Curie temperature for bcc Fe (1043 K). However, that of fcc FeH rapidly decreases with compression, possibly suggesting changes in the magnetic state at 300 K from FM to PM with local spin moment, which does not contradict previous Mössbauer measurements (Narygina et al., 2011).

Table S1. Thermodynamic parameters for thermal EoSs for FeH and Fe

	fcc FeH	fcc FeH	dhcp FeH	fcc Fe
Ref.	This study	Sakamaki et al. (2009)		Tsujino et al. (2013)
EoS at T_0	Vinet	3rd Birch–Murnaghan	3rd Birch–Murnaghan	3rd Birch–Murnaghan
Magnetic state[a]	NM	FM + PM	FM + PM	FM + PM
T_0 (K)	300	1273	300	1273
$V_{0,T0}$ (Å^3)	13.45(15)	14.15	12.80	12.257
$K_{0,T0}$ (GPa)	183(20)	182	112	111.5
$K'_{0,T0}$	3.84(37)	4	5.4	5.2
n	2	–[b]	2	1
γ_0	0.738(40)	–[b]	1.98	2.28
γ_∞	0.547(83)	–	–	–
q	–	–[b]	-0.6	-0.21
Θ_0 (K)	758	–[b]	340	340
Pressure range	P > 41 GPa	P < 21 GPa	P < 20 GPa	–

[a]NM, non magnetic state; PM, paramagnetic state with local spin moment

[b]Effect of temperature on the EoS is described by thermal pressure $\Delta P_{th} = P_{T0} + \alpha K_{T0} \times (T - T_0)$, where $\alpha K_{T0} = 1.8 \times 10^{-2}$ GPa/K.

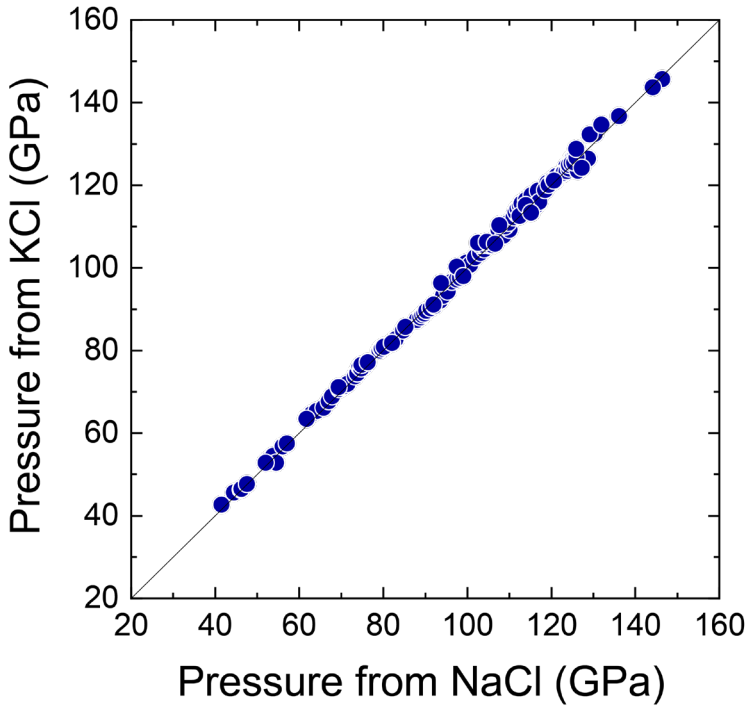

Figure S1. Comparison of pressures determined from an NaCl pressure marker (Dorogokpets & Dewaele, 2007) with those based on KCl (Tateno et al., 2019) in run #3.

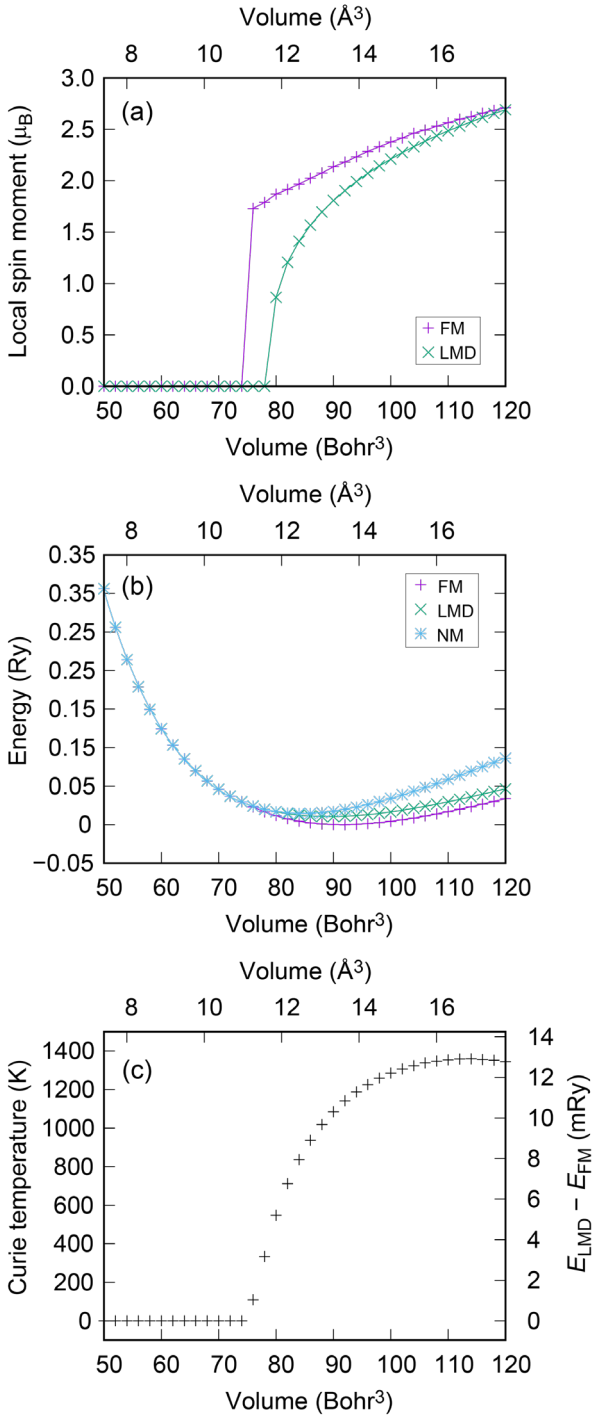

Figure S2. (a) Local spin moment of the FM (purple) and LMD (green) states of fcc FeH as a function of volume. Note that that of the LMD state is quenched at a volume larger than that for the FM state. (b) Total energy of the FM (purple), LMD (green), and NM (blue) states of fcc FeH as a function of volume. Symbols are first-principles results, and lines are fitting curves (see text). (c) Curie temperature of fcc FeH as a function of volume.

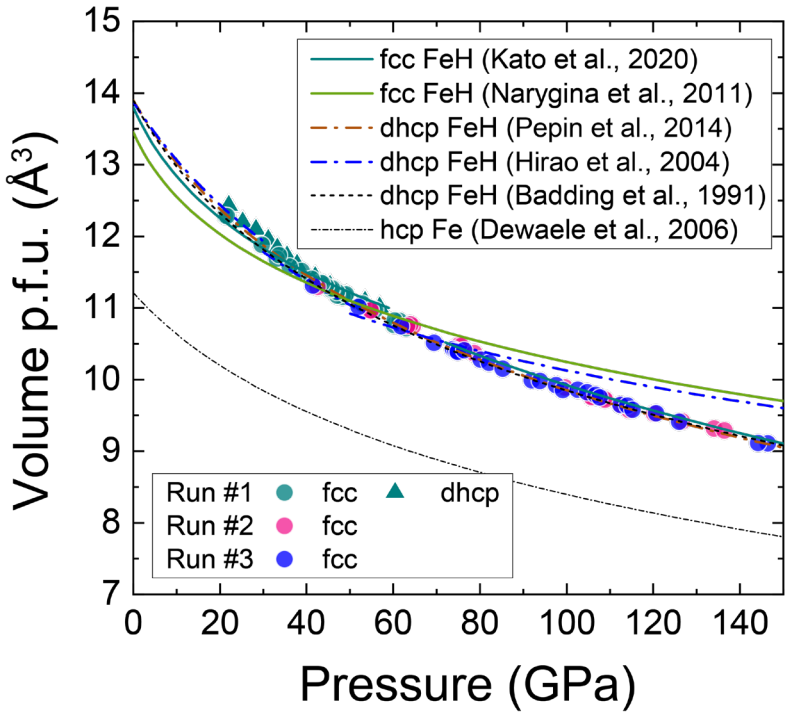

Figure S3. Comparison of the volume per formula unit of FeH obtained at 300 K in this study (circles, fcc; triangles, dhcp) with the compression curves for dhcp and fcc FeH reported by previous studies (Badding et al., 1991; Hirao et al., 2004; Narygina et al., 2011; Pépin et al., 2014; Kato et al., 2020). That of pure Fe is also shown (Dewaele et al., 2006).